water

MDPI

Article

Compound Impact of Storm Surge and Flood Characteristics in Coastal Area Based on Copula

Zhenglei Zhu [1], Wei Zhang [1,*] and Wenjin Zhu [2]

[1] College of Harbor, Coastal and Offshore Engineering, Hohai University, Nanjing 210098, China; zhenglei.zhu@hhu.edu.com
[2] School of Civil and Ocean Engineering, Jiangsu Ocean University, Lianyungang 222000, China; zhucius@jou.edu.cn
* Correspondence: zhangweihhu@126.com

Abstract: In low-lying coastal areas, the interplay of various factors including precipitation, river flow, and storm surge can lead to greater influence on floods when they occur simultaneously. The copula method was used in this study to investigate the bivariate flood risk of compounding storm surge and river discharge events in the Pearl River Delta (PRD). Our results indicate that while the correlation between storm surge and flood peak (S-Q) was weak, there was a strong dependence between the pairs of storm surge–flood volume (S-V) and storm surge–flood duration (S-D). For these three pairs, the Clayton copula was the optimal function for S-Q, while the Frank copula was the optimal function for S-V and S-D, respectively. When the flood volume exceeds 2.0×10^4 m^3/s and the flood duration is more than 10 days, the bivariate hydrologic risk for S-V and S-D is observed to decrease rapidly. Furthermore, the failure probability (FP) would be underestimated when the combined impact of river flow and storm surge is ignored in coastal flood risk assessment. Such bivariate hydrologic risk analysis implies that when determining design values in coastal flood risk assessment, the combined impact of river flow and storm surge should be taken into account.

Keywords: compound flood; statistical model; coastal-estuarine region; copula; storm surge; bivariate distribution; joint risk

Citation: Zhu, Z.; Zhang, W.; Zhu, W. Compound Impact of Storm Surge and Flood Characteristics in Coastal Area Based on Copula. *Water* **2024**, *16*, 270. https://doi.org/10.3390/w16020270

Academic Editor: Chin H Wu

Received: 15 December 2023
Revised: 9 January 2024
Accepted: 10 January 2024
Published: 12 January 2024

1. Introduction

Floods, the most common hazard globally [1], concern many water-related agencies. They have resulted in significant economic and social impacts in the past [2], posing increasing risks to both humans and the environment [3]. The threats are expected to rise, especially in coastal regions [4–6]. Coastal flooding, often referred to as compound flooding, arises from various factors: river inflows, tides, rainfall, wind, and oceanic events like upwellings, eddies, and storms [7,8]. Flooding may be more severe from extreme or compound events than from a single event if these drivers occur simultaneously or successively [2,9]. Even if the individual events are not extreme, their combined effect can be significant [9–11]. To accurately assess flood risks in these areas, we must evaluate the interdependence of hydrologic variables. Flood risk is a crucial factor to take into account when planning water facility improvements. It is required as a design standard [12–14] for hydraulic buildings, city drainage networks, dam management, and flood threat mapping [15]. However, because of their shifting character and the complex relationship of tidal and basin processes, it is difficult to evaluate flood risk in estuaries since the interplay between hydrologic variables remains poorly understood [16].

Traditional flood risk estimation relies on univariate flood frequency analysis [17,18]. The link between percentiles and non-exceedance opportunities (return periods) can be determined with this analysis. This estimation does not fully assess flood severity and occurrence because flood, based on river discharge data, is usually featured by peak, volume, and duration which is viewed as a multivariate phenomenon [19,20]. Research on flood frequency analysis would have significant impacts on the design of hydraulic infrastructure, disaster, and flood prevention. Specifically, a lot of attention has been attracted by multivariate flood risk analysis due to its comprehensive assessment of flood events. Consequently, copula theory has been integrated into recent flood risk analysis. This theory identifies the associations of two or more random variables, known as multivariate distribution functions. Copula functions offer an advantage over traditional multivariate hydrologic models because they separate the processes of determining marginal distributions and multivariate dependence. This gives practitioners greater freedom to select marginal and joint distribution functions [21,22]. Prior studies on floods primarily emphasized the combined distribution of flood peaks, volumes, and durations [23,24]. However, many of these studies assumed that hydrologic variables follow the same marginal distribution function [25]. Yet, hydrologic variables are interdependent and do not typically share the same marginal distribution. Mahmoudi et al. and Xu et al. [26,27] evaluated the compound effects of storm surges and precipitation on a coastal city's flood risk. Both studies highlighted that the combined impacts of surges and precipitation far exceed their individual effects; this is often overlooked in current flood defense designs. This combined effect and relationship between precipitation and storm surge has previously been investigated by Svensson and Jones [28]. These studies emphasize that univariate flood frequency analysis falls short when assessing extreme events caused by interconnected random variables [29–32]. But until now, to our knowledge, limited research has explored the compound impacts between storm surges and flood variables in coastal areas for distinct pair combinations.

Beyond flood frequency, recent studies [8,33–35] have introduced the concept of FP to quantify hydrologic event risks. They argue that the return period (RP) inadequately represents the risk throughout the whole project lifetime. Read and Vogel [33] highlighted that solely relying on an average RP is misleading as it disregards the planning scope. Serinaldi [36] argued that assessing FP throughout a project's design lifespan provides a more comprehensive risk evaluation. Xu et al. [24] used copulas to quantify the joint hydrologic risk of flood peak–volume–duration in the Wei River. Moftakhari et al. [8] use the concept of "failure probability" to assess compound flood risks caused by river discharge and water level under varying sea level rise scenarios. Such investigations show that the FP is an appropriate instrument for compound flood risk analysis. Nevertheless, no prior research has employed FP in bivariate hydrologic risk analysis, specifically for storm surge and flood variables.

China does not yet have a thorough regional analysis of the risks associated with compound flooding. Over 12% of China's population lives in low-lying coastal areas (elevation < 10 m), which make up 2% of the country's total geographical area [37,38]. Meanwhile, coastal hazards such as tropical cyclones and storm surges impact these areas frequently [39]. Between 1989 and 2014, coastal flooding led to over 4376 deaths and USD 71 billion in direct losses in China [40]. Such incidents have the potential to virtually destroy all of their assets in a few years and to halt city growth for years or even decades. It is expected that the increased precipitation brought on by climate change would increase the cost of safeguarding these communities from storms and rising sea levels. Furthermore, as coastal areas continue to urbanize, many coastal and estuarine communities are likely to face significant flood risk issues [16,41]. Many studies conducted in the last few decades have attempted to comprehend extreme hydrologic occurrences in the Pearl River Delta (PRD). For example, Zhang et al. [42] revealed the spatial and temporal patterns of the extreme water level in the PRD region. The importance of consideration of hydrological alterations in the evaluation of flood risk was emphasized by Zhang et al. [43]. Zhang et al. [44] assessed flood frequency in the PRD with the distribution of generalized extreme value (GEV). However, although research attempts on flood occurrence have been recorded, there are not many studies that examine the compound flood risk in the PRD.

Therefore, this study focuses for the first time on the analysis of storm surge and flood variables in the PRD utilizing long-term historical data. We address two key questions in this study: (1) what is the relationship between storm surge and flood characteristics, and

(2) how do the storm surge and flood characteristics affect the compound flood risk in the PRD? Joint probabilities for storm surge–flood peak (S-Q), storm surge–volume (S-V), and storm surge–duration (S-D) were quantified using copula methods. Additionally, we utilize FP to evaluate the variability in compound flood risk throughout the project's lifetime. The findings would offer a theoretical foundation for managing flood risk and serve as references for flood mitigation and other coastal city applications.

2. Data and Methods

2.1. Data Collection

The daily mean river discharge records for the PRD's Makou and Sanshui stations from 1961 to 2012 were collected for this study from China's hydrological yearbooks [39]. Additionally, we visually examined the river discharge time series and eliminated any erroneous spikey values. The PRD's critical gauging stations, Makou and Sanshui, are located on the west and north rivers, respectively, as Figure 1 illustrates. River discharge through Makou regulates the quantity of water that flows through the western distributaries of PRD, whereas river discharge through Sanshui controls the amount that flows through the northern distributaries. According to the findings of [45], the long-term trends of stream flow at Makou and Sanshui showed a significant downward and rising trend, respectively (Figure 2). These alterations are connected to the shift in Makou and Sanshui's streamflow ratio. Therefore, the river discharge summed from the two stations which becomes insignificant is used in this study. This is consistent with the negligible trend in the precipitation in the Pearl River catchment [46,47]. In situ observations of storm surge events in Hong Kong during 1961–2012 were collected from Hong Kong observatory (https://www.hko.gov.hk/sc/wservice/tsheet/pms/stormsurgedb.htm, accessed on 8 September 2022.). In Hong Kong, storm surge events come from the North Point and Quarry Bay stations, which are considered as the same station since the tidal records show no significant difference. Table 1 provides descriptive statistics for the examined variables: storm surge, flood peak (Q), flood volume (V), and flood duration (D). Sharp and right-tailed distributions can be used to represent the flood variables, according to the positive kurtosis and skewness values.

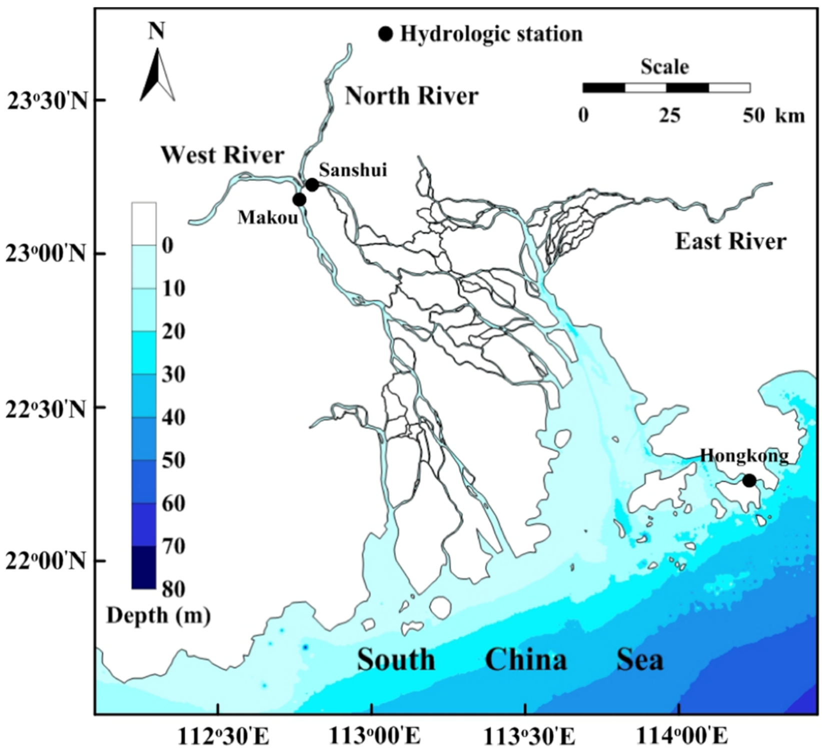

Figure 1. Map of the Pearl River Delta. Hydrological stations are indicated by solid dots.

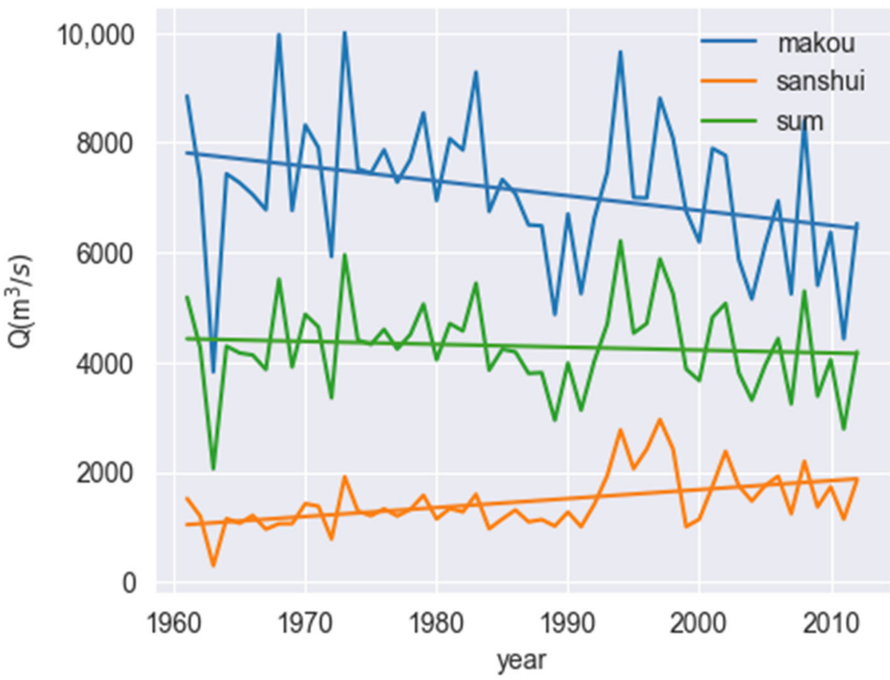

Figure 2. Time series of annual mean river discharge; the blue line denotes Makou discharge, the orange line denotes Sanshui discharge, and the green line denotes the sum discharge from both stations. Straight lines show the linear trends for the periods of 1961–2012.

Table 1. Statistical characteristics of storm surge and river discharge.

	Surge (m)	River Discharge		
		Q (m^3/s)	V (m^3)	D (Day)
mean	0.491	34,287	319,133	17.54
std	0.295	10,494	238,885	9.53
min	0.020	20,230	59,380	5
25%	0.310	27,820	159,620	11
50%	0.430	30,800	255,980	16
75%	0.585	40,150	387,050	22
max	1.340	62,400	1,027,330	48
skewness	1.153	1.1993	1.4458	1.1796
kurtosis	1.371	1.3439	1.7219	1.8128

2.2. POT Model

The Peak-Over-Threshold (POT) method, which involves selecting all values above a given threshold, has been historically employed in flood frequency analyses [48–50]. For the POT model, comprehensive operational guidelines were supplied by Lang et al. [51]. Before employing the POT model, two critical issues need addressing: (1) making sure the chosen peak series is independent, and (2) selecting a suitable threshold [52,53]. This study examined the independence of the peak series using the popular declustering method that was first proposed by the US Water Resources Council in 1976 [50,54]. To achieve this, consecutive flood events must fulfill two requirements:

$$\theta > 5 + ln\left(\frac{A}{1.609^2}\right) \text{ and } Q_{min} < \frac{3}{4} min(Q_1, Q_2) \quad (1)$$

where θ denotes the interval time between two consecutive peaks (days), A is the basin area (Km^2), Q_1 and Q_2 are two consecutive peak flows (m^3/s), and Q_{min} is the minimum intermediate flow (m^3/s).

On average, peak river discharges that occurred three times per year were extracted from the daily river discharge time series. This determines the threshold value of the river discharge as 19,700 m^3/s. Subsequently, we calculated the flood volume and duration for each flood event with river discharge surpassing the selected threshold (Figure 3). Additionally, the corresponding storm surges within each flood duration were selected.

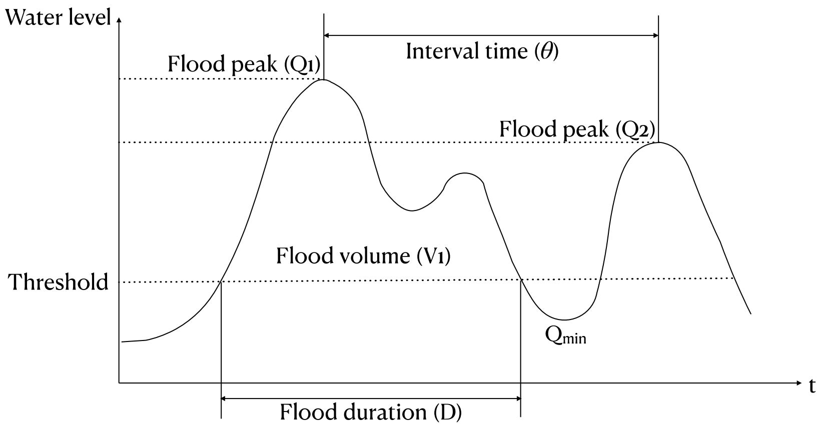

Figure 3. Typical flood hydrograph showing flood flow characteristics and the schematic diagram for separation of the successive flood events.

2.3. Copula Function

Copula functions enable flexible selection of the marginal distribution, which are extensively used in multivariate analysis. Copulas have recently been found to be used in the analysis of drought frequency [55,56], rainfall frequency [57], and flood frequency analysis [58]. Further details of copulas and their characteristics are available in [59,60]. The bivariate distribution is given by Equation (2) if there is a correlation between X_1 and X_2.

$$H(X_1, X_2) = C\left(F_{X_1}(x_1), F_{X_2}(x_2)\right) \tag{2}$$

where $H(X_1, X_2)$ represents the bivariate distribution function; C is a copula function; $F_{X_1}(x_1) = P(X_1 \leqslant x_1)$ and $F_{X_2}(x_2) = P(X_2 \leqslant x_2)$ stand for marginal distribution. An independent joint distribution function (Equation (3)) would be employed to explain this bivariate distribution if X_1 and X_2 are independent.

$$H(X_1, X_2) = F_{X_1}(x_1) \cdot F_{X_2}(x_2) \tag{3}$$

Utilizing the Kolmogorov–Smirnov (K-S) test, the effectiveness of the marginal distributions was assessed. It is a free test for nonparametric probability distributions [61]. The K-S test statistic measures the greatest vertical distance between the expected and observed distributions [22] which is described as follows:

$$D_n = max\left|F_{exp}(x) - F_{obs}(x)\right| \tag{4}$$

where $F_{exp}(x)$ stands for the expected distribution, $F_{obs}(x)$ denotes the observed distribution.

To construct the joint distribution of river discharge and storm surge, four typical bivariate copula functions (Table 2) are employed in this study. We utilize two criteria: Akaike's Information Criterion (AIC) and the Bayesian Information Criterion (BIC) to determine which copula has the best fit. Below are the *AIC* and *BIC* formulas:

$$AIC = -2lnL + 2k \tag{5}$$

$$BIC = -2lnL + ln(n)k \tag{6}$$

where lnL is the maximum likelihood estimation function, n is the number of compound events, and k is the number of parameters in the copula.

Table 2. Bivariate Archimedean copulas definitions.

Name of Copula	Generator	Bivariate Copula $C_\theta(u,v)$	Parameter θ
Clayton	$\frac{1}{\theta}\left(t^{-\theta}-1\right)$	$\left(u^{-\theta}+v^{-\theta}-1\right)^{-1/\theta}$	$\theta \in [-1,\infty)$
Gumbel	$(-log(t))^{\theta}$	$e^{[-((-log(u))^{\theta}+(-log(v))^{\theta})^{1/\theta}]}$	$\theta \in [1,\infty)$
Frank	$-log\left(\frac{e^{-\theta t}-1}{e^{-\theta}-1}\right)$	$-\frac{1}{\theta}log\left[1+\frac{(e^{-\theta u}-1)(e^{-\theta v}-1)}{e^{-\theta}-1}\right]$	$\theta \in R \setminus \{0\}$
Joe	$-log\left(1-(1-t)^{\theta}\right)$	$1-\left[(1-u)^{\theta}+(1-v)^{\theta}-(1-u)^{\theta}(1-v)^{\theta}\right]^{1/\theta}$	$\theta \in [1,\infty)$

2.4. Joint Return Period (JRP)

A hazard's return period (RP) is equal to the average interarrival time between occurrences divided by the exceedance probability. The term "joint return period (JRP)" describes the typical interval between natural hazard events. In compound flood analyses, the JRP of the driving mechanisms typically considers two risk scenarios: an extreme threshold being exceeded by one driver (OR scenario) or both drivers surpassing their respective thresholds (AND scenario). Situations when at least one driver surpasses the threshold are indicated by the OR-joint probability $P(X_1 > x_1 \cup X_2 > x_2)$, and the associated OR-joint RP is indicated by Equation (7).

$$\begin{aligned} T_{X_1X_2}^{OR} &= \frac{M_t}{P(X_1>x_1 \cup X_2>x_2)} \\ &= \frac{M_t}{1-P(X_1<x_1 \cup X_2<x_2)} \\ &= \frac{M_t}{1-C(u_1,u_2)} \end{aligned} \quad (7)$$

where $C(u_1, u_2)$ is the joint distribution, and M_t is the hazard event's average recurrence time, usually expressed in years. It is calculated by dividing the total number of incidents by the duration of the events.

The AND-joint probability $P(X_1 > x_1 \cap X_2 > x_2)$ refers to both drivers occuring at the same time, and its return period is represented by the following:

$$\begin{aligned} T_{X_1X_2}^{AND} &= \frac{M_t}{P(X_1>x_1 \cap X_2>x_2)} \\ &= \frac{M_t}{1-P(X_1<x_1)-P(X_2<x_2)+P(X_1<x_1 \cap X_2<x_2)} \\ &= \frac{M_t}{1-F_{X_1}(x_1)-F_{X_2}(x_2)+C(u_1,u_2)} \end{aligned} \quad (8)$$

where $F_{X_1}(x_1)$ and $F_{X_2}(x_2)$ are the marginal distribution.

2.5. Failure Probability

Hydrologic risk is evaluated by FP, defined as the likelihood of a potential flood event taking place at least once over the lifespan of a project [8,22,35,62]. The equation for calculating the FP is as follows:

$$P = 1 - \prod_{i=1}^{N} F(X) = 1 - \prod_{i=1}^{N} (1 - \frac{M_t}{T}) \quad (9)$$

where $F(x)$ represents the non-exceedance probability, N is the hydraulic structure's design life, and T is the time it takes for a flooding event to recur.

In practical flood management, characterizing a flood event requires considering multiple parameters, such as storm surge and flood duration, rather than just one aspect like storm surge alone. For instance, severe property losses could result from a flood event involving a storm surge and a long flood duration, whereas a short-period event with a storm surge might simply produce a flash flood. As a result, determining the compound flood risk is essential for developing flood mitigation plans and putting nonstructural safety measures into place. In our study, the bivariate risk is defined using the JRP in the AND scenario as described below:

$$FP = 1 - (1 - \frac{M_t}{T_{X_1X_2}^{AND}})^N \tag{10}$$

3. Results

3.1. Dependence and Seasonal Variation

It is essential to correctly model the dependency of extremes while estimating in multivariate frequency analysis [63,64]. Therefore, we must first answer the question of whether there are any dependencies between storm surge and flood variables before we can analyze the joint probability. Three grouped (S-Q, S-V, S-D) data were displayed in Figure 4. Diagonal histograms in the figure aid in identifying each variable's distribution, kurtosis, and skewness. The figure categorizes the time gap between storm surge and flood variables into three intervals: 0–5 days (short), 5–15 days (medium), and over 15 days (long). We find that 68.57% compound events have short day deltas (yellow points), while the longer day deltas (blue points) typically correspond to stronger grouped variables.

To assess the suitability of a copula model for the aforementioned goal, we calculated Kendall's tau (τ) and Spearma's rho (ρ), in addition to Pearson's linear correlation (r). These measures identified the dependence structure among S-Q, S-V, and S-D pairs, and are shown in Table 3. The S-D pair exhibits the strongest correlation with Pearson's r = 0.403, Kendall's τ = 0.289, and Spearman's ρ = 0.413. The pair of S-V also exhibits significant correlation with Pearson's r = 0.332, Kendall's τ = 0.288, and Spearman's ρ = 0.401. Conversely, the lowest correlation is seen between storm surge and flood peak. To graphically depict this dependence, the Chi-plot and Kendall plot (Figure 5) were employed in this study. Usually, a traditional scatter plot of the raw data is employed in conjunction with the Chi-plot graphic tool. It can be useful in detecting the associations within random samples from continuous bivariate distributions. The Kendall plot, or K-plot for short, is an additional alternate display that uses the probability plot concept for dependence discovery. The benefit of K-plots is that they can be easily extended to the multivariate environment.

Rank scatter plots, Chi-plots, and K-plots are used in Figure 5 to graphically illustrate the dependence for the pairs of S-Q, S-V, and S-D. In the Chi-plots, the horizontal coordinate λ represents the distance from each point to the sample's median, while the vertical coordinate χ indicates the deviation from the null hypothesis (the two variables are independent), represented by the gray dotted line. If the null hypothesis is correct, approximately 95% of the χ values would fall between two red dashed lines. It is evident that most of the points in the scatter plot for S-D (S-V) lie near the main diagonal, suggesting a high-rank dependence between storm surge and flood duration (or flood volume). The situation is less pronounced for the S-Q pair due to their weaker dependence. The use of 'control limits' ($\pm C_p/\sqrt{n}$) as the 'confidence band' in Chi-plot was suggested by Fisher and Switzer [65]. The cp values in this case are 1.54, 1.78, and 2.18, which correspond to p values of 0.9, 0.95, and 0.99, respectively. It is evident that there are dependent relationships between S-D and S-V pairs because the region inside the confidence band denotes complete independence. The majority of S-Q points, in contrast, fall inside the confidence interval, denoting a modest degree of dependence between these driving factors. When it comes to K-plots, the region bounded by the diagonal and the curve represents the dependent relationship. The dependence is comparatively weaker when the points are close to the diagonal, but it is large when the points are close to the curve. The findings show that the S-D's points are closest to the curve, followed by the S-V points, but the S-Q's points are close to the diagonal, indicating that the S-Q combination has a mildly positive correlation. The diagrams' results are in line with the estimated correlation coefficients, which show that the degrees of correlation between storm surge, flood peak, volume, and duration are in the order S-D > S-V > S-Q.

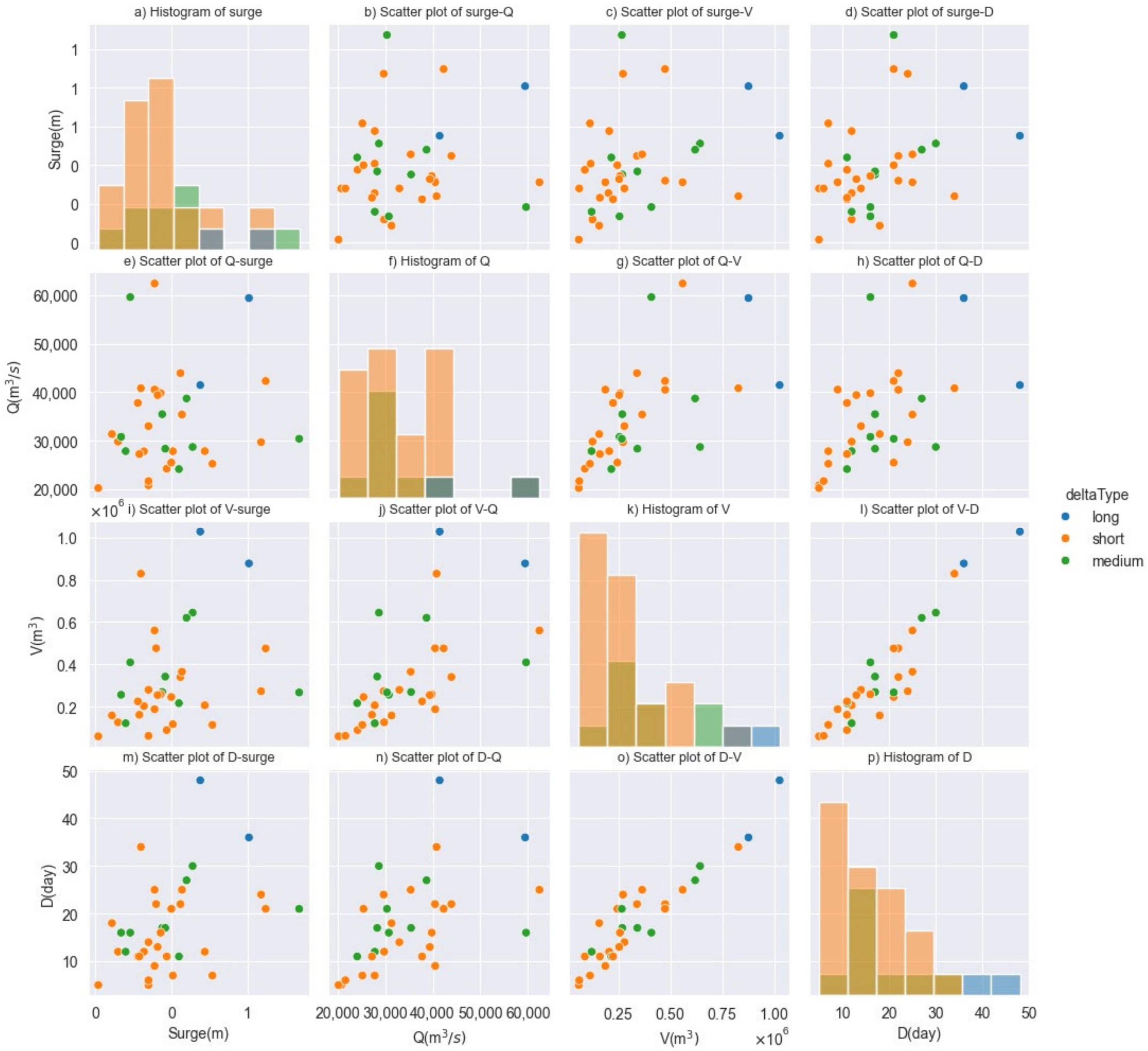

Figure 4. Scatter plot for storm surge and flood variables. Different colored points indicate different day deltas between the flood peak and storm surge. Orange dots indicate 0–5 days, green dots indicate 5–15 days, and blue dots indicate 15 days or less. On the diagonal are histograms.

Table 3. Dependence evaluations among flooding variables.

Pair	Pearson's r	Kendall's τ	Spearman's ρ
S-Q	0.139	0.078	0.125
S-V	0.332	0.288	0.401
S-D	0.403	0.289	0.413

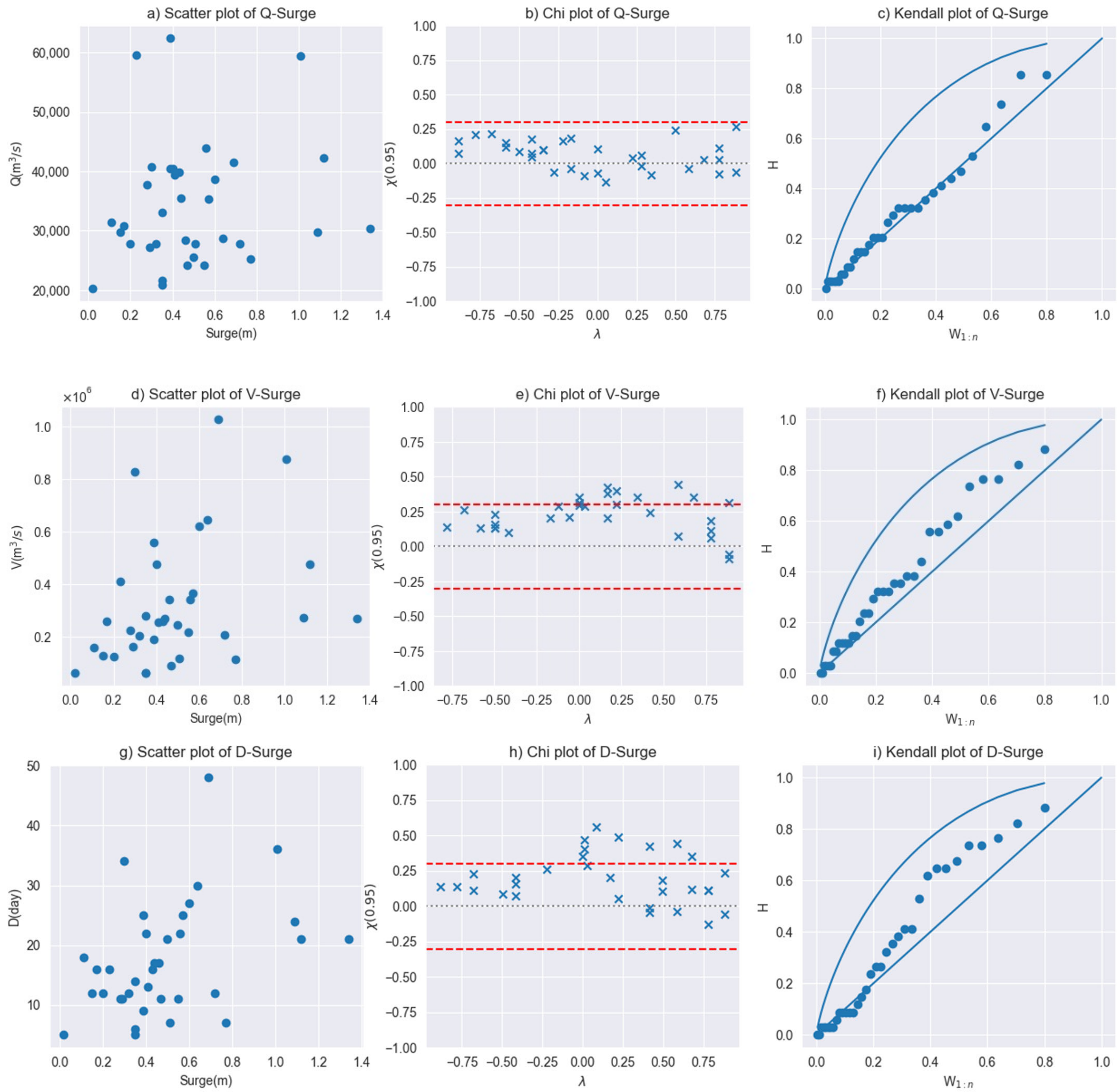

Figure 5. Graphical representation of strength of dependence using scatter plot, chi-plot, and Kendall plot. In the middle column, the cross points are the pair of (λ, χ), the λ represents the distance from each point to the sample's median, the χ indicates the deviation from the null hypothesis (the two variables are independent), and the zone between the two red dash lines denotes complete independence. In the right column, the dot is the pair of ($W_{1:n}$, H), the curve denotes perfect positive dependence, and the diagonal denotes independence.

Note that not all of the dependence structure of the joint distribution can be captured by scalar dependence measures like ρ, τ, and r. Therefore, since storm surge and flood variables have been shown to be positively correlated, we now deal with the issue of determining their copula.

To better understand the timing of events with relatively higher compound flood potential, the influence of seasons is investigated. For the seasonal analysis, We assessed the compound flood potential for each month by calculating the number of compound events. Both storm surge and flood peak exhibits significant seasonal variations (Figure 6). Affected by the summer monsoon precipitation from the Northwest Pacific Subtropical High and TCs from the western North Pacific, most of the flood peak events occurred from May to August, and the storm surge events mostly occurred from June to October. The compound events are also obtained from Figure 6. It can be detected that the compound events were more likely to occur from June to August in the PRD.

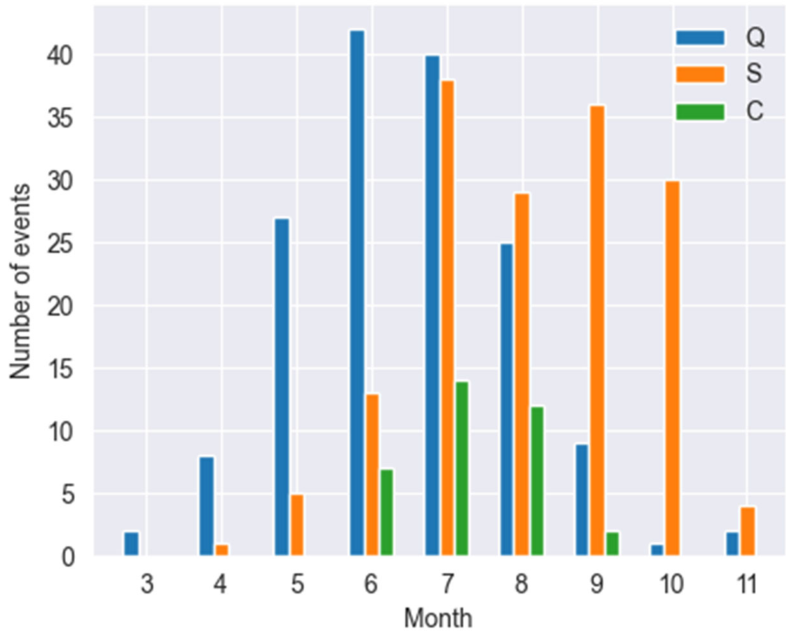

Figure 6. Flood and storm surge events from 1961 to 2012, whereas the blue bar denotes the number of flood peak events, the orange bar denotes the number of storm surge events, and the green bar denotes the number of compound events.

3.2. Marginal Distribution

The suggested study's flow chart is shown in Figure 7. The copula method provides flexibility in selecting the marginal and joint distribution functions. As indicated in Table 1, all variables exhibit positive skewness. Seven skewed distribution functions were used in this study: Gamma, GEV, Genpareto, Gumbel, Lognorm, Pearson3, and Weibull, to estimate the marginal distributions for storm surge, flood peak, flood volume, and flood duration. To assess how well the seven models performed, the K-S test (Equation (4)) was used. This test aims to calculate the deviation between the expected distribution and the observed distribution. Table 4 presents the parameters of probability density functions (PDFs) for each of the seven distributions. All parameters were derived using the maximum likelihood estimation method. The K-S test results were used to identify the most effective techniques for measuring the marginal distributions of storm surge, flood peak, flood volume, and flood duration. Figure 8 shows the fitted seven distribution functions for the four variables, where the empirical denotes the observations' probabilities. The cumulative distribution functions (CDFs) for storm surge and flood duration from the seven marginal distribution functions demonstrate strong agreement with the observed data. The K-S test results indicate that for surge, Q, V, and D, the best-performing models are the Gumbel, Gamma, Genpareto, and Genextreme distributions, respectively, as evidenced by the minimum K-S values. The superior performance of our suggested approaches is indicated by the associate p-value of the K-S test, which is greater than 0.05.

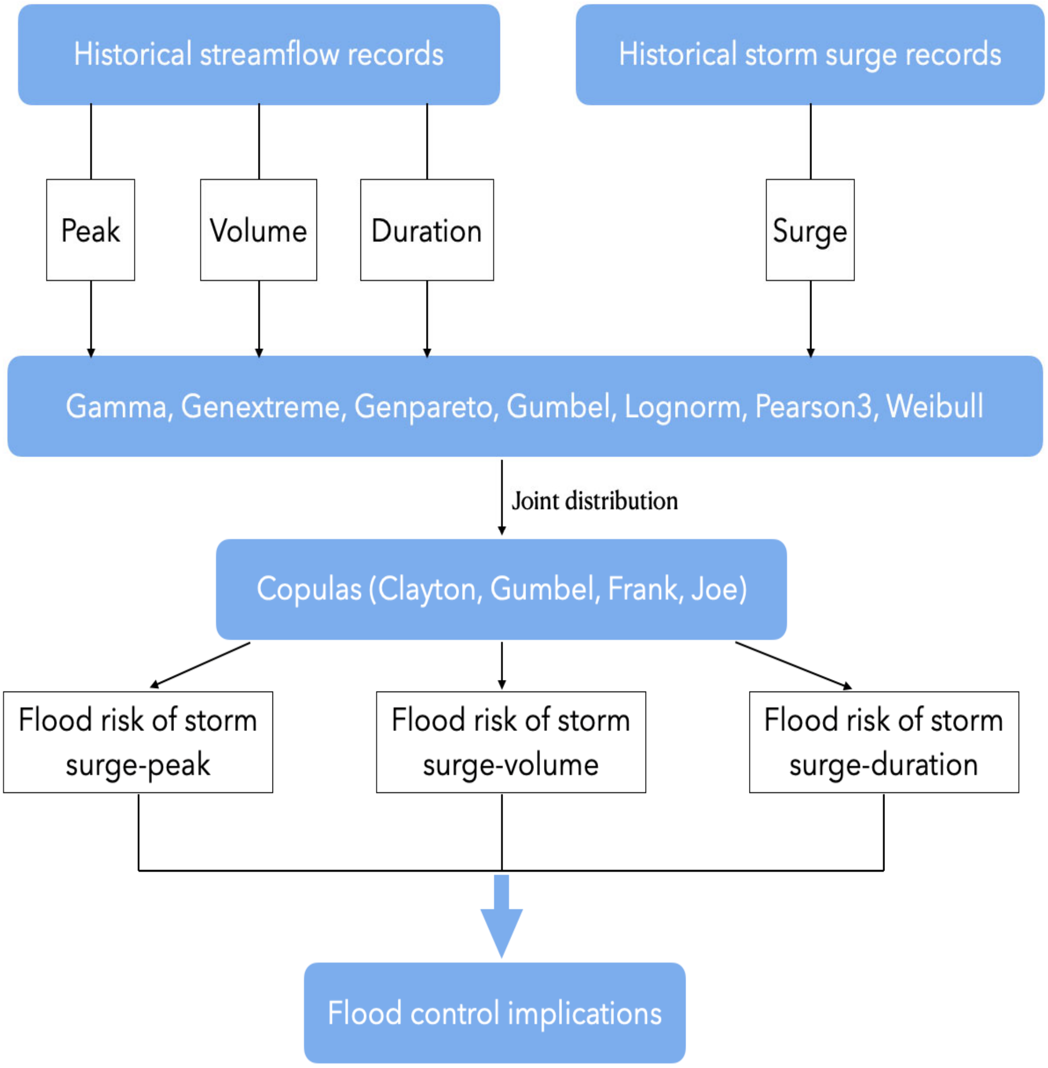

Figure 7. The flow chart of the proposed study.

Table 4. Parameters of marginal distribution functions.

Variable	Distribution	c	loc	Scale	K-S	p-Value
Surge	Gamma	4.076	−0.085	0.141	0.077	0.977
	Genextreme	−0.029	0.358	0.218	0.068	0.993
	Genpareto	−0.469	0.020	0.680	0.173	0.222
	Lognorm	0.373	−0.258	0.698	0.071	0.989
	Gumbel	**NaN**	**0.362**	**0.220**	**0.064**	**0.997**
	Pearson3	0.991	0.491	0.285	0.077	0.977
	Weibull	1.447	0.099	0.440	0.075	0.981
Flood peak (Q)	**Gamma**	**2.033**	**19,093**	**7471**	**0.088**	**0.925**
	Genextreme	−7.382	20,230	0.760	0.705	0.000
	Genpareto	−1.078	−126	67402	0.306	0.002
	Lognorm	11.706	20,230	0.974	0.679	0.000
	Gumbel	NaN	29,725	7519	0.096	0.877
	Pearson3	1.403	34,286	10,654	0.088	0.925
	Weibull	1.395	19,837	15,808	0.094	0.891

Table 4. *Cont.*

Variable	Distribution	c	loc	Scale	K-S	*p*-Value
Flood volume (V)	Gamma	0.841	59,380	272,645	0.177	0.196
	Genextreme	−8.815	59,380	1.351	0.692	0.000
	Genpareto	**−0.138**	**59,346**	**295,485**	**0.113**	**0.722**
	Lognorm	9.439	59,380	1.496	0.767	0.000
	Gumbel	NaN	219,386	155,162	0.150	0.372
	Pearson3	2.097	302,643	255,024	0.147	0.402
	Weibull	0.953	59,380	255,074	0.124	0.606
Flood duration (D)	Gamma	1.809	4.022	7.473	0.123	0.621
	Genextreme	**−0.086**	**13.036**	**6.744**	**0.094**	**0.887**
	Genpareto	−0.296	4.605	16.455	0.167	0.255
	Lognorm	0.489	−1.463	16.906	0.095	0.880
	Gumbel	NaN	13.357	6.993	0.103	0.815
	Pearson3	1.487	17.543	10.052	0.123	0.621
	Weibull	1.342	4.565	14.076	0.124	0.613

Note: Best estimate is shown in bold.

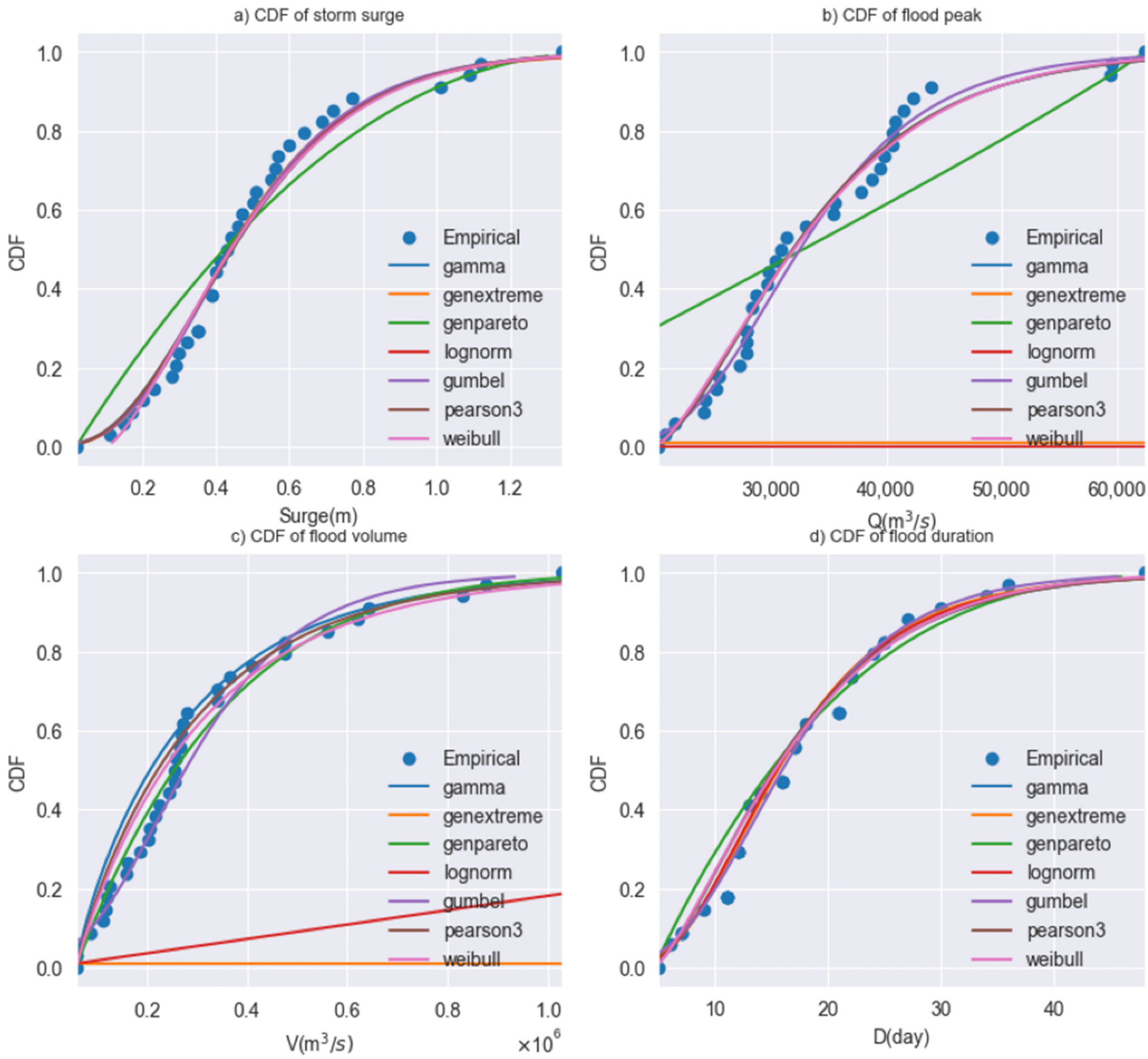

Figure 8. Comparison between theoretical and empirical probabilities. CDF denotes cumulative distribution function.

3.3. Joint Distribution

Four Archimedean families of copulas—Clayton, Frank, Gumbel, and Joe—were used in this study to describe the relationship between storm surge and flood variables. (refer to Table 2). There are various copulas for modeling the dependence between storm surge and flood variables. Therefore, to determine which of these copulas is best, AIC and BIC were employed and the copula with the lowest values was selected. A smaller AIC or BIC result corresponds to a good fit, which is indicated by a greater log-likelihood [66]. The copulas' properties and statistical test results are shown in Table 5. In summary, the four Archimedean copulas function satisfactorily when modeling the pairs S-Q, S-V, and S-D. Overall, based on the results from Table 5, the Clayton copula appears most suitable for modeling the storm surge and flood peak, while the parameters for S-V and S-D are best estimated by the Frank copula.

Table 5. Parameters and criteria selection of copula model.

Pair	Name of Copula	Parameter	Log-Likelihood	AIC	BIC
Surge-Q	**Clayton**	**0.349**	**1.727**	**−1.454**	**0.101**
	Gumbel	1.109	0.512	0.976	2.531
	Frank	0.865	0.344	1.313	2.868
	Joe	1.094	0.225	1.550	3.106
Surge-V	Clayton	0.263	2.359	−2.717	−1.162
	Gumbel	1.265	2.304	−2.608	−1.053
	Frank	**2.734**	**3.111**	**−4.222**	**−2.666**
	Joe	1.258	1.079	−0.158	1.397
Surge-D	Clayton	0.500	2.283	−2.566	−1.011
	Gumbel	1.307	2.605	−3.209	−1.654
	Frank	**2.709**	**3.257**	**−4.513**	**−2.958**
	Joe	1.388	1.899	−1.798	−0.243

Note: Best estimate is shown in bold.

Following copula selection, we constructed the bivariate distribution function by considering the chosen marginal distributions. Figures 9–11 display the empirical and theoretical joint distribution functions for S-Q, S-V, and S-D. The black dotted lines in Figures 9–11 represent the empirical joint probabilities. They are derived from $C(u,v) = 1/n\sum_{i=1}^{n} I(R_i/(n-1) \leqslant u,\ S_i/(n-1) \leqslant v)$, where $u,v \in [0,1]$, Ri, and Si denote the ranks of the ordered sample, and $I(A)$ is the indicator function for event A. The results indicate a strong agreement between the theoretical and empirical copulas. We calculate the joint probabilities for various RP based on these iso-probability curves, as shown in Table 6.

Table 6. The joint return periods (year).

T	T_{SQ}^{AND}	T_{SV}^{AND}	T_{SD}^{AND}	T_{SQ}^{OR}	T_{SV}^{OR}	T_{SD}^{OR}
5	56.90	30.23	30.42	2.61	2.73	2.72
10	225.00	111.84	112.61	5.11	5.23	5.23
20	894.82	428.96	432.03	10.11	10.24	10.24
50	5573.23	2611.35	2630.72	25.11	25.24	25.24
100	22,267.03	10,352.21	10,429.82	50.11	50.24	50.24

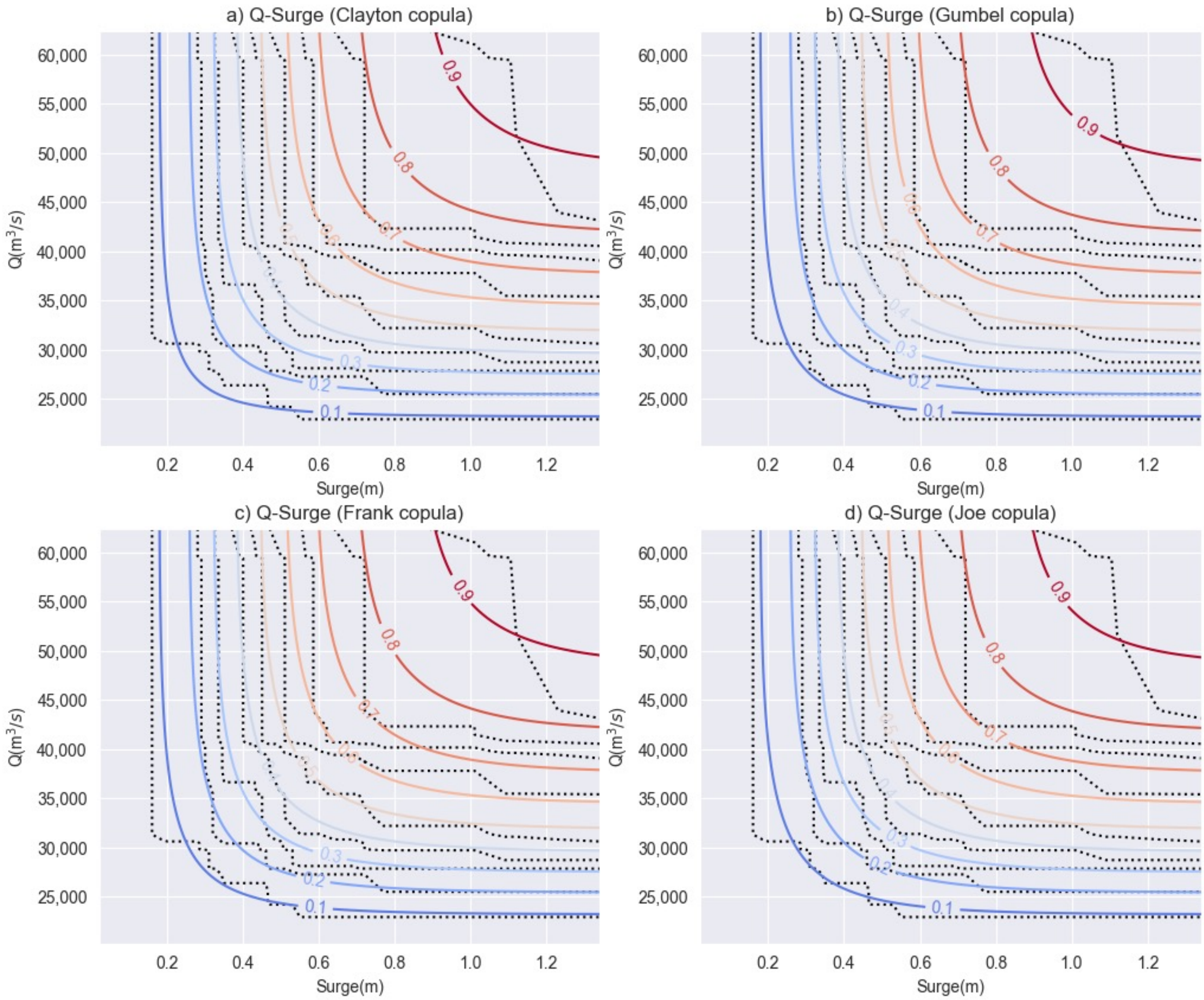

Figure 9. Comparison between the empirical (dotted lines) and theoretical (solid lines) joint probability for storm surge and flood peak.

3.4. Bivariate RP

RP is a typical way to describe natural hazards and risks. The RP represents the time interval between events of the same intensities. But this definition does not imply that such an event occurs only once within the given interval. Actually, it quantifies the yearly probability of the event, regardless of when the last comparable occurrence happened. The concurrent probabilities of storm surge and flood variable combinations offer deeper insights for flood events, aiding practical flood mitigation and management. Bivariate RP encompasses both OR-joint and AND-joint RPs. Equations (7) and (8) can be used to derive the JRPs based on the chosen copula functions. Table 6 presents the AND- and OR-JRPs. Generally, the OR-joint return period is significantly shorter than both the univariate and AND-joint return periods. Specifically, the OR-JRPs for storm surge and flood variables are nearly half that of the marginal RP. This suggests that the univariate analysis might not capture the complete risk associated with various flood hazard factors. For example, with a marginal RP of 50 years, the OR-JRP for storm surge and flood volume is around 25 years, while the AND-JRP is about 2611 years. This outcome indicates that overlooking the combined effects of storm surge and flood variables can misrepresent coastal flood risks, potentially leading to underestimations. Therefore, bivariate RP analysis offers a more thorough and logical assessment than univariate RP analysis. Figure 12 displays contour plots representing AND and OR-JRPs of storm surge and flood variables.

Compared with univariate RP, AND and OR-JRP can either expand or reduce dangerous regions [34], which would precisely characterize a dangerous event. Consequently, they are suitable for specific application requirements. For instance, in flood engineering design, if a hazardous event is when both heavy river discharge and storm tide events simultaneously occur, the AND-joint RP is recommended.

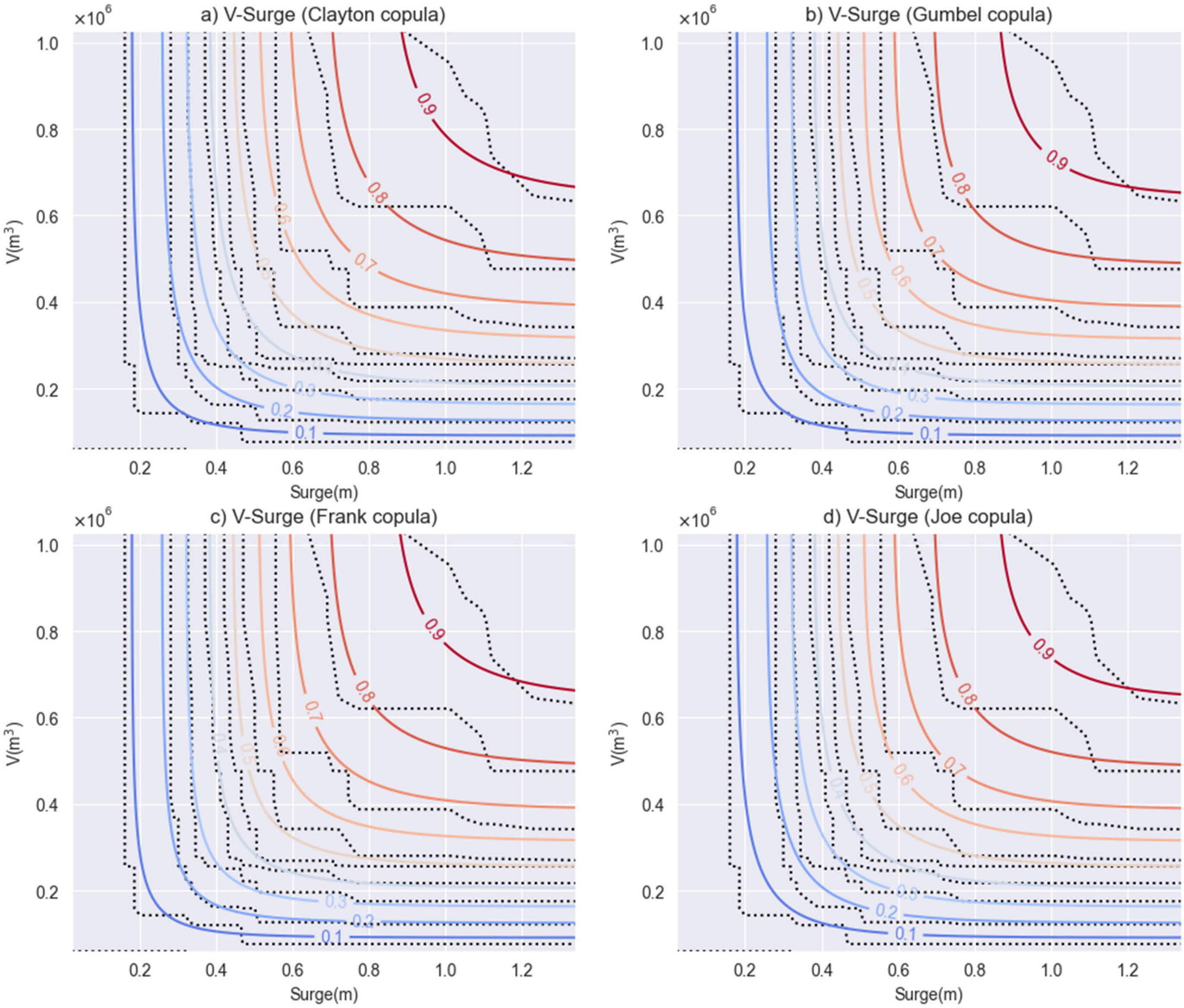

Figure 10. Comparison between the empirical (dotted lines) and theoretical (solid lines) joint probability for storm surge and flood volume.

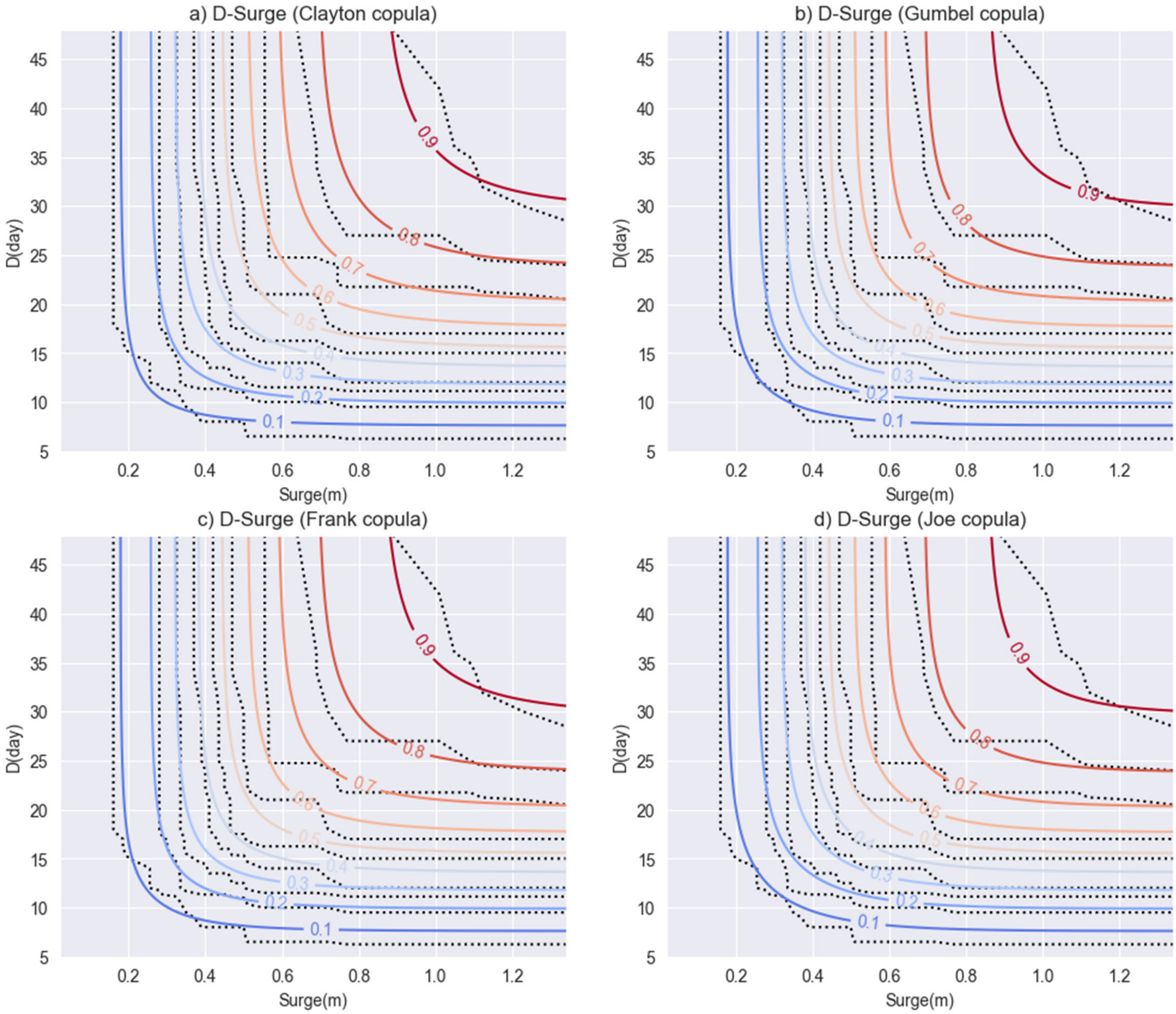

Figure 11. Comparison between the empirical (dotted lines) and theoretical (solid lines) joint probability for storm surge and flood duration.

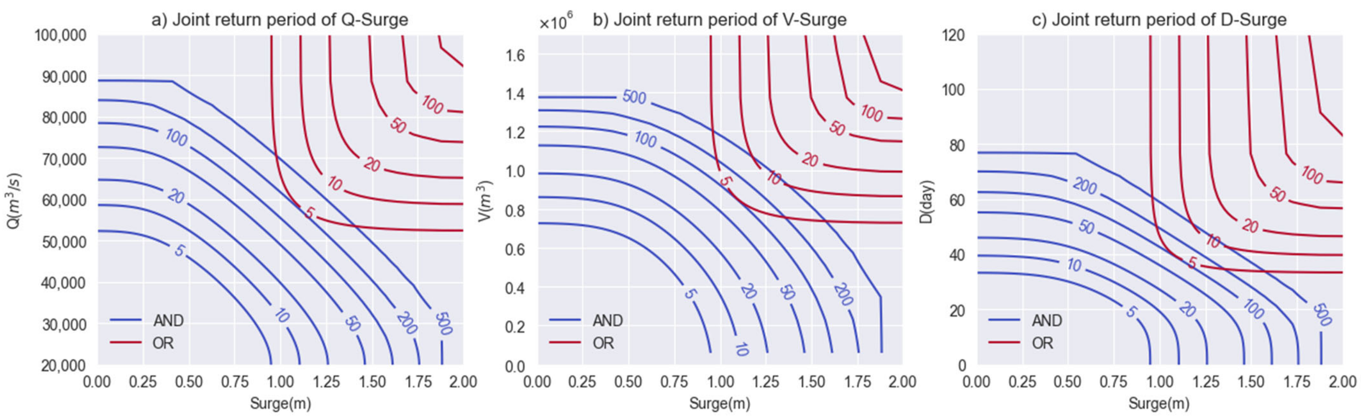

Figure 12. The contour plot of the joint return period (year).

3.5. Compound Flood Risk

Figure 13 illustrates the bivariate flood risk in the PRD under different storm surge and flood duration scenarios, which is measured by FP. Throughout the course of a project, this probability represents the chance that a possible flood event will occur at least once [8,23]. The blue and green curves in this figure represent the FP under the condition of univariate and bivariate (storm surge and flood duration), respectively. The figure demonstrates that (1) a higher RP corresponds with lower univariate and bivariate flood risks. (2) The increased servicing time for hydraulic facilities would raise the flood risk. For example, for a 100-year univariate RP event, the FP stands at 0.033 for a 10-year service time and increases to 0.154 for a 50-year one. This suggests that RP is not strictly linked to a planning period, and thus cannot define the likelihood of an event within a project's lifetime [23]. (3) The FP of bivariate events is higher than that of univariate events, indicating that there is an underestimation of FP when the compounding effect is overlooked. (4) If the association between storm surge and flood duration is ignored, the FP of a flood event will be overestimated (red line in Figure 13). This agrees well with what Moftakhari et al. [8] found. It suggests that when analyzing their FPs, the correlation between storm surge and flood variables should be considered.

Figure 14 depicts the compound flood risk associated with flood variables and storm surge. The blue, green, and red lines in Figure 14 represent three scenarios for the variables: 50-year, 100-year, and 150-year RPs, respectively. The marginal distribution is used to estimate variables in the three return period scenarios. Additionally, based on local conditions, three service time scenarios (which represent the hydraulic structures' design lives, denoted by n in Equations (9) and (10)) were established. In this research, we assume the service times for hydraulic facilities are 30, 50, and 100 years. As we can see, with an increase in hydraulic facility service time, the compound flood risk values would increase, and it would decrease with the increase in the RP of flood variables and storm surge. This indicates that the compound flood risk would be reduced by raising the hydraulic facilities' design standards. Furthermore, the hydrologic risk drops rapidly when variables (on the x-axis) surpass a specific threshold, and when the variables exceed a higher value, the hydrological risk becomes smaller and decreases slowly. For example, there is a rapid decline in compound flood risk when the storm surge exceeds 0.3 m for a 30-year service time and 0.5 m for a 100-year service time. Moreover, the compound flood risk reduces gradually when the design storm surge surpasses 1.3 m for 30 years and 1.5 m for 100 years. The findings indicate that the water level should be designed between 0.3 m and 1.5 m above the astronomical tide level. Considering the flood peak (Q) paired with three return periods of storm surge, risk values start declining when Q is beyond 2×10^4 m^3/s and 3×10^4 m^3/s for 30 and 100 years of service time, respectively. The compound flood risk would decrease slowly and to a lesser extent when the Q exceeds 6×10^4 m^3/s and 7×10^4 m^3/s for 30 and 100 years of service time. According to the results, the flood peak should be planned to be at least 2×10^4 m^3/s and lower than 7×10^4 m^3/s. Paired with three storm surge return periods, the compound flood risk drops notably as flood volume exceeds 2×10^5 m^3/s and 5×10^5 m^3/s for 30 and 100 years service time, respectively. It shrinks significantly (almost to 0) as the flood volume surpasses 10×10^5 m^3/s and 12×10^5 m^3/s in the service time of 30 and 100 years. These findings imply that the areas designated for flood diversion would be planned with a flood volume that is at least larger than 2×10^5 m^3/s and lower than 12×10^5 m^3/s. The compound flood risk for flood duration and three storm surge RPs can be easily obtained, the same as the one for flood volume. Based on the results, it can be concluded that the compound flood risk would dramatically decline for flood duration longer than 10 and 20 days, corresponding to 30 and 100 years of service time, respectively. Accordingly, a flood that happened close to the PRD would most likely endure for at least 10 days and no more than 60. This analysis serves as a guideline for sustainable flood engineering planning and design in coastal regions.

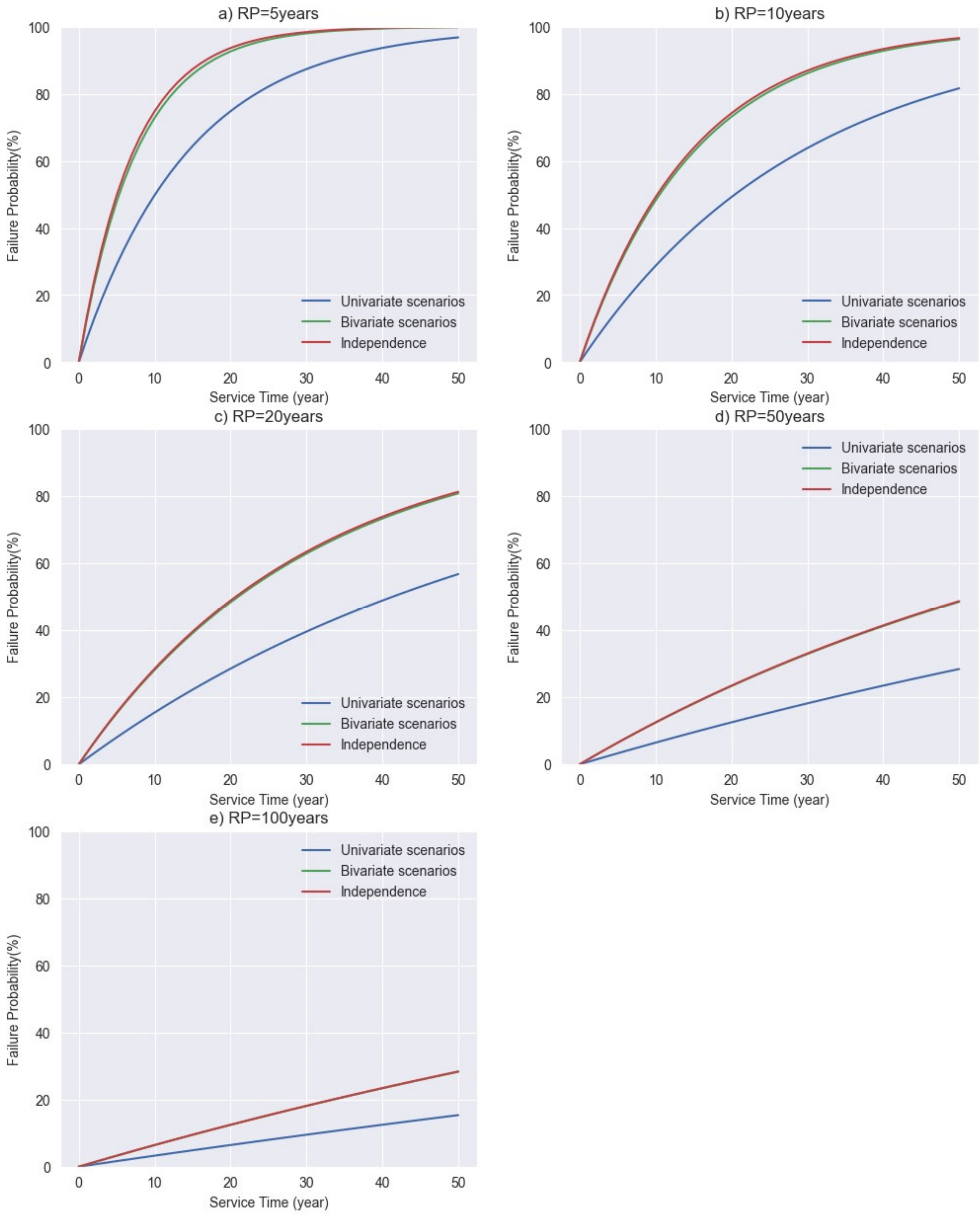

Figure 13. The bivariate flood risk of storm surge and flood duration in different RPs. The estimated failure probability derived from the univariate and bivariate OR situations is displayed in the blue and green curves, respectively. The red curve represents the failure probability when the unreasonable assumption of independence is used.

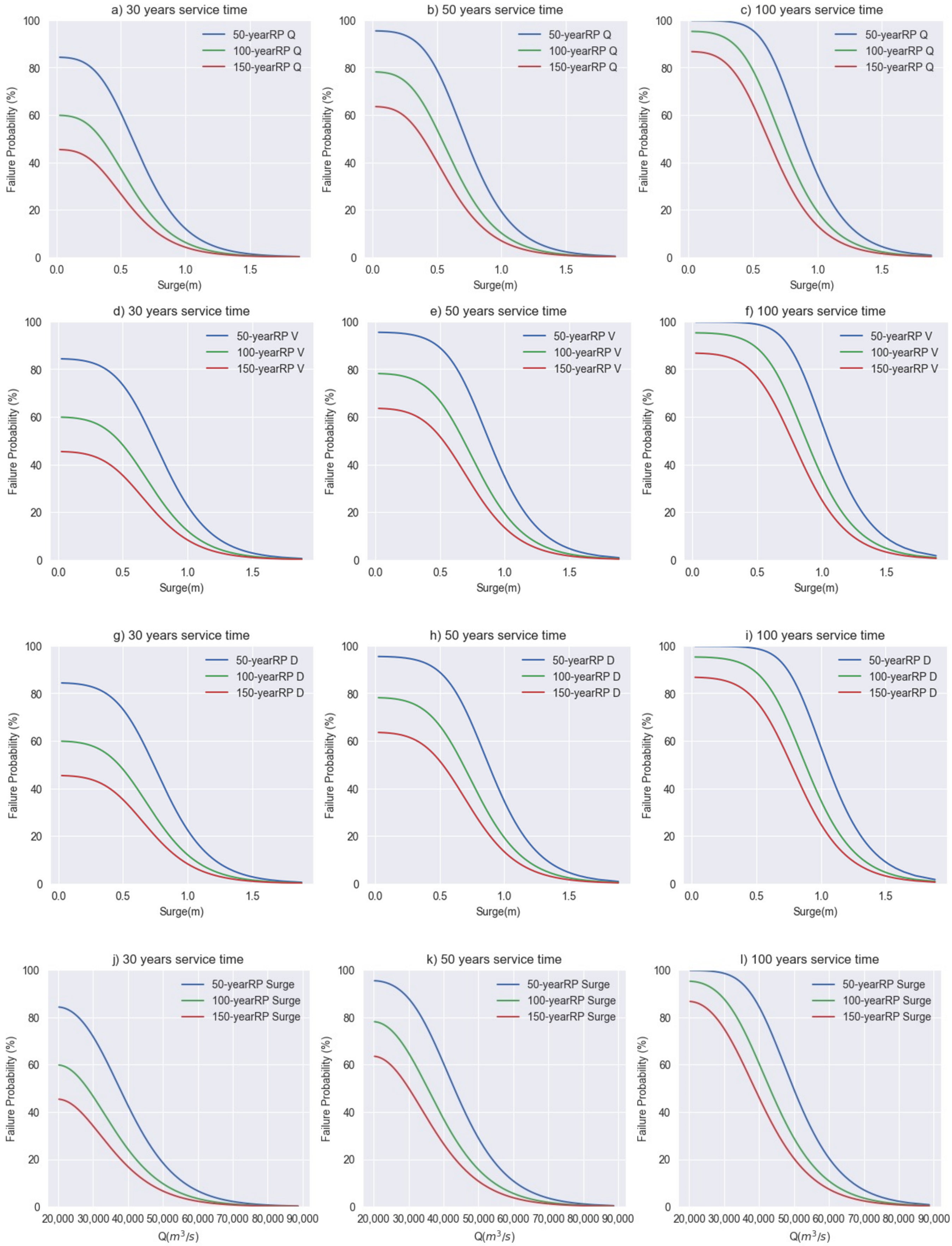

Figure 14. *Cont.*

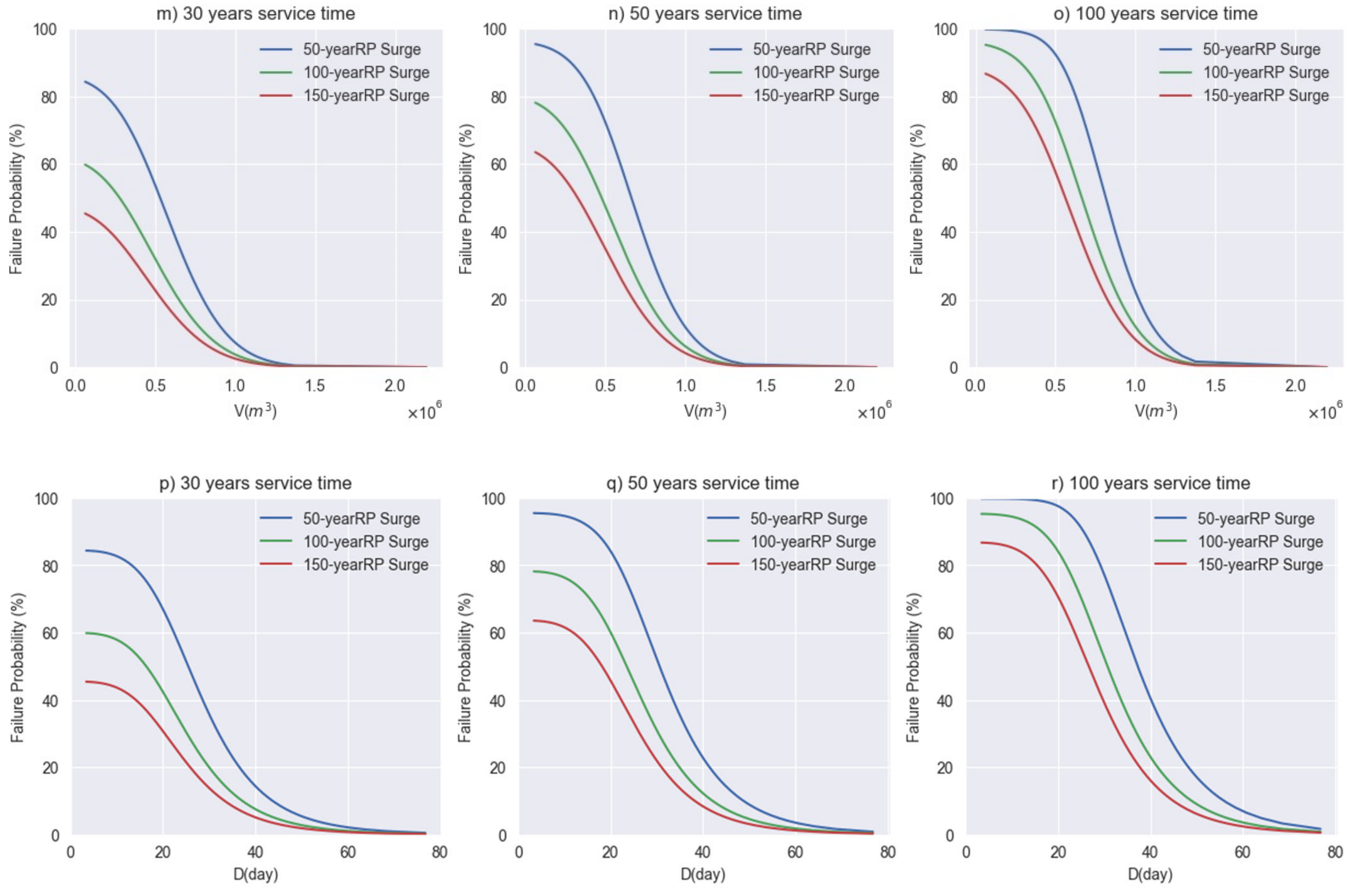

Figure 14. The variation in the bivariate flood risk. The first three rows with the change in storm surge in different designed Q, V, and D, respectively. The last three rows with the change in Q, V and D in different designed storm surges.

4. Conclusions and Discussions

In this study, a comprehensive analysis was conducted to explore the joint impacts of storm surge and river flow on the PRD. Through graphical tests and rank correlations between storm surge and flood variables (i.e., flood peak, volume, and duration), it was discovered that the dependence between these factors was statistically significant. Using the copula method, a compound flood risk analysis was performed. Firstly, the JRPs of compound flood for S-Q, S-V, and S-D were established. Then, the compound flood risk was defined based on the JRP. The obtained copulas were tested through AIC and BIC to determine whether they were statistically satisfied. Finally, the compound flood risks for S-Q, S-V, and S-D were finally identified.

The compound flood risk analysis was conducted using storm surge data and daily river discharge data from 1961 to 2012. We find that, during a flood, 68.57% compound events occur within 5 days (yellow points), while the longer day deltas (blue points) typically correspond to stronger grouped variables. The correlation results show that storm surge is highly correlated with flood volume and duration. But the correlation with flood peak was much smaller. The Frank copula proved to be best for assessing the joint distributions of the S-V and S-D pairs among the four Archimedean copulas, whereas the Clayton copula is acknowledged as a correct function for the joint distribution of the S-Q pair. The univariate RP is greater than the OR-JRP and less than the AND-JRP. It demonstrates that flood hazards, which are influenced by a variety of factors, are difficult to comprehend since univariate analysis provides little information. Particularly, the AND-JRP for S-Q is probably two times that of the S-V and S-D pairs due to the lowest dependence. The compound flood risk would rise with the increase in the hydraulic facilities' lifespan. The FP of univariate events is less than that of bivariate events, indicating an underestimation of FPs due to ignoring the compounding impacts of flood drivers. According to the compound flood risk assessment for S-D, compound flood events would last at least ten days. However, as the duration of a flood rises, the risk of such a compound flood decreases considerably. Similarly, the compound flood risk for S-V suggests that a flood would normally be accompanied by a volume of at least 2×10^5 m^3/s, and the compound flood risk reduces slightly as the flood volume exceeds 10×10^5 m^3/s. These compound flood risks could help with the design of hydraulic facilities, as well as flood prevention and mitigation.

The method created in this study to analyze compound floods could be used for other coastal towns or regions. However, the impact of anthropogenic forcing, geological, and geomorphological characteristics on compound flood is overlooked, which may have an impact on our findings. These influences include inconsistent riverbed changes between periods and river channels caused by sand mining and sediment flux fluctuations, as well as river flow management through dam control to reduce flood and drought risk. As a result, research on these driving factors should be an important part in the development of future flood design standards. Furthermore, climate change-related flooding could be an attractive topic for future research.

Author Contributions: Methodology, Z.Z. and W.Z. (Wei Zhang); Software, W.Z. (Wenjin Zhu); Formal analysis, Z.Z.; Investigation, W.Z. (Wenjin Zhu); Writing—original draft, Z.Z.; Writing—review & editing, W.Z. (Wei Zhang). All authors have read and agreed to the published version of the manuscript.

Funding: This research was jointly funded by "National Natural Science Foundation of China" (NSFC, Project NoS. 42006157), The Belt and Road Special Foundation of the National Key Laboratory of Water Disaster Prevention (2020492111).

Data Availability Statement: The river discharge data is available from the China's hydrological yearbooks. Storm surge data is obtained from the Hong Kong observatory [https://www.hko.gov.hk/sc/wservice/tsheet/pms/stormsurgedb.htm].

Conflicts of Interest: The authors declare no conflict of interest.

References

1. Kundzewicz, Z.W.; Kanae, S.; Seneviratne, S.I.; Handmer, J.; Nicholls, N.; Peduzzi, P.; Mechler, R.; Bouwer, L.M.; Arnell, N.; Mach, K.; et al. Flood risk and climate change: Global and regional perspectives. *Hydrol. Sci. J.* **2014**, *59*, 1–28. [CrossRef]
2. Hemmati, M.; Ellingwood, B.R.; Mahmoud, H.N. The Role of Urban Growth in Resilience of Communities Under Flood Risk. *Earth's Futur.* **2020**, *8*, e2019EF001382. [CrossRef]
3. Muis, S.; Verlaan, M.; Winsemius, H.C.; Aerts, J.C.J.H.; Ward, P.J. A global reanalysis of storm surges and extreme sea levels. *Nat. Commun.* **2016**, *7*, 11969. [CrossRef]
4. Hallegatte, S.; Green, C.; Nicholls, R.J.; Corfee-Morlot, J. Future flood losses in major coastal cities. *Nat. Clim. Change* **2013**, *3*, 802–806. [CrossRef]
5. Lian, J.; Xu, H.; Xu, K.; Ma, C. Optimal management of the flooding risk caused by the joint occurrence of extreme rainfall and high tide level in a coastal city. *Nat. Hazards* **2017**, *89*, 183–200. [CrossRef]
6. Zscheischler, J.; Martius, O.; Westra, S.; Bevacqua, E.; Raymond, C.; Horton, R.M.; van den Hurk, B.; AghaKouchak, A.; Jézéquel, A.; Mahecha, M.D.; et al. A typology of compound weather and climate events. *Nat. Rev. Earth Environ.* **2020**, *1*, 333–347. [CrossRef]
7. Wahl, T.; Jain, S.; Bender, J.; Meyers, S.D.; Luther, M.E. Increasing risk of compound flooding from storm surge and rainfall for major US cities. *Nat. Clim. Chang.* **2015**, *5*, 1093–1097. [CrossRef]
8. Moftakhari, H.R.; Salvadori, G.; AghaKouchak, A.; Sanders, B.F.; Matthew, R.A. Compounding effects of sea level rise and fluvial flooding. *Proc. Natl. Acad. Sci. USA* **2017**, *114*, 9785–9790. [CrossRef]
9. Zscheischler, J.; Westra, S.; Van Den Hurk, B.J.J.M.; Seneviratne, S.I.; Ward, P.J.; Pitman, A.; AghaKouchak, A.; Bresch, D.N.; Leonard, M.; Wahl, T.; et al. Future climate risk from compound events. *Nat. Clim. Chang.* **2018**, *8*, 469–477. [CrossRef]
10. Leonard, M.; Westra, S.; Phatak, A.; Lambert, M.; van den Hurk, B.; McInnes, K.; Risbey, J.; Schuster, S.; Jakob, D.; Stafford-Smith, M. A compound event framework for understanding extreme impacts. *WIREs Clim. Chang.* **2014**, *5*, 113–128. [CrossRef]
11. Chao, S.R.; Ghansah, B.; Grant, R.J. An exploratory model to characterize the vulnerability of coastal buildings to storm surge flooding in Miami-Dade County, Florida. *Appl. Geogr.* **2021**, *128*, 102413. [CrossRef]
12. *GB 50015-2019*; Standard for Design of Building Water Supply and Drainage. China Planning Press: Beijing, China, 2019.

13. *JTS 145-2-2013*; Code of Hydrology for Sea Harbour. China Communication Press: Beijing, China, 2013.
14. *GB/T 51015-2014*; Code for Design of Sea Dike Project. China Planning Press: Beijing, China, 2014.
15. Chebana, F.; Dabo-Niang, S.; Ouarda, T.B.M.J. Exploratory functional flood frequency analysis and outlier detection. *Water Resour. Res.* **2012**, *48*, 4514. [CrossRef]
16. Petroliagkis, T.I.; Voukouvalas, E.; Disperati, J.; Bidlot, J. Joint Probabilities of Storm Surge, Significant Wave Height and River Discharge Components of Coastal Flooding Events. European Commission-JRC Technical Reports, Italia. 2016. Available online: https://publications.jrc.ec.europa.eu/repository/handle/JRC100839 (accessed on 8 September 2022).
17. Bevacqua, E.; Maraun, D.; Haff, I.H.; Widmann, M.; Vrac, M. Multivariate statistical modelling of compound events via pair-copula constructions: Analysis of floods in Ravenna (Italy). *Hydrol. Earth Syst. Sci.* **2017**, *21*, 2701–2723. [CrossRef]
18. Lan, M.; Gardoni, P.; Luo, R.; Zhu, J.; Lo, S. Risk-driven statistical modeling for hurricane-induced compound events: Design event implementation for industrial areas subjected to coastal floods and winds. *Ocean Eng.* **2022**, *251*, 111159. [CrossRef]
19. Adamson, P.T.; Metcalfe, A.V.; Parmentier, B. Bivariate extreme value distributions: An application of the Gibbs Sampler to the analysis of floods. *Water Resour. Res.* **1999**, *35*, 2825–2832. [CrossRef]
20. Qin, X.S.; Lu, Y. Study of Climate Change Impact on Flood Frequencies: A Combined Weather Generator and Hydrological Modeling Approach. *J. Hydrometeorol.* **2014**, *15*, 1205–1219. [CrossRef]
21. Qin, X.S. Assessing environmental risks through fuzzy parameterized probabilistic analysis. *Stoch. Environ. Res. Risk Assess.* **2012**, *26*, 43–58. [CrossRef]
22. Fan, Y.R.; Huang, W.W.; Huang, G.H.; Huang, K.; Li, Y.P.; Kong, X.M. Bivariate hydrologic risk analysis based on a coupled entropy-copula method for the Xiangxi River in the Three Gorges Reservoir area, China. *Theor. Appl. Clim.* **2016**, *125*, 381–397. [CrossRef]
23. Ganguli, P.; Reddy, M.J. Probabilistic assessment of flood risks using trivariate copulas. *Theor. Appl. Clim.* **2013**, *111*, 341–360. [CrossRef]
24. Xu, Y.; Huang, G.H.; Fan, Y.R. Multivariate flood risk analysis for Wei River. *Stoch. Environ. Res. Risk Assess.* **2017**, *31*, 225–242. [CrossRef]
25. Zhang, L.; Singh, V.P. Bivariate Flood Frequency Analysis Using the Copula Method. *J. Hydrol. Eng.* **2006**, *11*, 150–164. [CrossRef]
26. Mahmoudi, M.H.; Najafi, M.R.; Singh, H.; Schnorbus, M. Spatial and temporal changes in climate extremes over northwestern North America: The influence of internal climate variability and external forcing. *Clim. Chang.* **2021**, *165*, 14. [CrossRef]
27. Xu, H.; Tian, Z.; Sun, L.; Ye, Q.; Ragno, E.; Bricker, J.; Mao, G.; Tan, J.; Wang, J.; Ke, Q.; et al. Compound flood impact of water level and rainfall during tropical cyclone periods in a coastal city: The case of Shanghai. *Nat. Hazards Earth Syst. Sci.* **2022**, *22*, 2347–2358. [CrossRef]
28. Svensson, C.; Jones, D.A. Dependence between sea surge, river flow and precipitation in south and west Britain. *Hydrol. Earth Syst. Sci.* **2004**, *8*, 973–992. [CrossRef]
29. Chebana, F.; Ouarda, T. Multivariate quantiles in hydrological frequency analysis. *Environmetrics* **2011**, *22*, 63–78. [CrossRef]
30. Ward, P.J.; Couasnon, A.; Eilander, D.; Haigh, I.D.; Hendry, A.; Muis, S.; I E Veldkamp, T.; Winsemius, H.C.; Wahl, T. Dependence between high sea-level and high river discharge increases flood hazard in global deltas and estuaries. *Environ. Res. Lett.* **2018**, *13*, 084012. [CrossRef]
31. Chao, Z.; Wang, H.; Hu, S.; Wang, M.; Xu, S.; Zhang, W. Permeability and porosity of light-weight concrete with plastic waste aggregate: Experimental study and machine learning modelling. *Constr. Build. Mater.* **2024**, *411*, 134465. [CrossRef]
32. Chao, Z.; Shi, D.; Fowmes, G. Mechanical behaviour of soil under drying–wetting cycles and vertical confining pressures. *Environ. Geotech.* **2023**, *63*, 101–109. [CrossRef]
33. Read, L.K.; Vogel, R.M. Reliability, return periods, and risk under nonstationarity. *Water Resour. Res.* **2015**, *51*, 6381–6398. [CrossRef]
34. Xu, H.; Xu, K.; Lian, J.; Ma, C. Compound effects of rainfall and storm tides on coastal flooding risk. *Stoch. Environ. Res. Risk Assess.* **2019**, *33*, 1249–1261. [CrossRef]
35. Pirani, F.J.; Najafi, M.R. Characterizing compound flooding potential and the corresponding driving mechanisms across coastal environments. *Stoch. Environ. Res. Risk Assess.* **2023**, *37*, 1943–1961. [CrossRef]
36. Serinaldi, F. Dismissing return periods! *Stoch. Environ. Res. Risk Assess.* **2015**, *29*, 1179–1189. [CrossRef]
37. Liu, J.; Wen, J.; Huang, Y.; Shi, M.; Meng, Q.; Ding, J.; Xu, H. Human settlement and regional development in the context of climate change: A spatial analysis of low elevation coastal zones in China. *Mitig. Adapt. Strat. Glob. Chang.* **2015**, *20*, 527–546. [CrossRef]
38. Fang, J.; Lincke, D.; Brown, S.; Nicholls, R.J.; Wolff, C.; Merkens, J.-L.; Hinkel, J.; Vafeidis, A.T.; Shi, P.; Liu, M. Coastal flood risks in China through the 21st century—An application of DIVA. *Sci. Total. Environ.* **2020**, *704*, 135311. [CrossRef] [PubMed]
39. Zhang, C.; Yin, K.; Shi, X.; Yan, X. Risk assessment for typhoon storm surges using geospatial techniques for the coastal areas of Guangdong, China. *Ocean Coast. Manag.* **2021**, *213*, 105880. [CrossRef]
40. Fang, J.; Liu, W.; Yang, S.; Brown, S.; Nicholls, R.J.; Hinkel, J.; Shi, X.; Shi, P. Spatial-temporal changes of coastal and marine disasters risks and impacts in Mainland China. *Ocean Coast. Manag.* **2017**, *139*, 125–140. [CrossRef]
41. Du, S.Q.; He, C.; Huang, Q.; Shi, P. How did the urban land in floodplains distribute and expand in China from 1992-2015? *Environ. Res. Lett.* **2018**, *13*, 034018. [CrossRef]

42. Changjiang River Water Resource Committee. *Hydrological Yearbooks of the People's Republic of China*; Changjiang River Water Resource Committee: Beijing, China, 2019. (In Chinese)
43. Zhang, Q.; Gu, X.; Singh, V.P.; Xiao, M. Flood frequency analysis with consideration of hydrological alterations: Changing properties, causes and implications. *J. Hydrol.* **2014**, *519*, 803–813. [CrossRef]
44. Zhang, W.; Cao, Y.; Zhu, Y.; Wu, Y.; Ji, X.; He, Y.; Xu, Y.; Wang, W. Flood frequency analysis for alterations of extreme maximum water levels in the Pearl River Delta. *Ocean Eng.* **2017**, *129*, 117–132. [CrossRef]
45. Feng, X.; Zhang, W.; Zhu, Z.; Chevuturi, A.; Chen, W. Variability and changes in Pearl River Delta water level: Oceanic and atmospheric forcing perspectives. *J. Hydrometeorol.* **2021**, *22*, 2407–2422. [CrossRef]
46. Zhao, Q.; Liu, Q.; Ma, L.; Ding, S.; Xu, S.; Wu, C.; Liu, P. Spatiotemporal variations in rainfall erosivity during the period of 1960–2011 in Guangdong Province, southern China. *Theor. Appl. Climatol.* **2017**, *128*, 113–128. [CrossRef]
47. Deng, S.; Chen, T.; Yang, N.; Qu, L.; Li, M.; Chen, D. Spatial and temporal distribution of rainfall and drought characteristics across the Pearl River basin. *Sci. Total. Environ.* **2018**, *619–620*, 28–41. [CrossRef]
48. Ribatet, M.; Sauquet, E.; Grésillon, J.-M.; Ouarda, T.B.M.J. A regional Bayesian POT model for flood frequency analysis. *Stoch. Environ. Res. Risk Assess.* **2007**, *21*, 327–339. [CrossRef]
49. Zadeh, S.M.; Durocher, M.; Burn, D.H.; Ashkar, F. Pooled flood frequency analysis: A comparison based on peaks-over-threshold and annual maximum series. *Hydrol. Sci. J.* **2019**, *64*, 121–136. [CrossRef]
50. Zhang, Q.; Zhang, L.; She, D.; Wang, S.; Wang, G.; Zeng, S. Automatic procedure for selecting flood events and identifying flood characteristics from daily streamflow data. *Environ. Model. Softw.* **2021**, *145*, 105180. [CrossRef]
51. Lang, M.; Ouarda, T.; Bobée, B. Towards operational guidelines for over-threshold modeling. *J. Hydrol.* **1999**, *225*, 103–117. [CrossRef]
52. Mazas, F.; Hamm, L. A multi-distribution approach to POT methods for determining extreme wave heights. *Coast. Eng.* **2011**, *58*, 385–394. [CrossRef]
53. Bernardara, P.; Mazas, F.; Kergadallan, X.; Hamm, L. A two-step framework for over-threshold modelling of environmental extremes. *Nat. Hazards Earth Syst. Sci.* **2014**, *14*, 635–647. [CrossRef]
54. Durocher, M.; Zadeh, S.M.; Burn, D.H.; Ashkar, F. Comparison of automatic procedures for selecting flood peaks over threshold based on goodness-of-fit tests. *Hydrol. Process.* **2018**, *32*, 2874–2887. [CrossRef]
55. Xu, K.; Yang, D.; Xu, X.; Lei, H. Copula based drought frequency analysis considering the spatio-temporal variability in Southwest China. *J. Hydrol.* **2015**, *527*, 630–640. [CrossRef]
56. Abdi, A.; Hassanzadeh, Y.; Talatahari, S.; Fakheri-Fard, A.; Mirabbasi, R. Regional bivariate modeling of droughts using L-comoments and copulas. *Stoch. Environ. Res. Risk Assess.* **2017**, *31*, 1199–1210. [CrossRef]
57. Zhang, Q.; Singh, V.P.; Li, J.; Jiang, F.; Bai, Y. Spatio-temporal variations of precipitation extremes in Xinjiang, China. *J. Hydrol.* **2012**, *434–435*, 7–18. [CrossRef]
58. Li, F.; Zheng, Q. Probabilistic modelling of flood events using the entropy copula. *Adv. Water Resour.* **2016**, *97*, 233–240. [CrossRef]
59. Nelsen, R.B. *An Introduction to Copulas*; Springer: Berlin/Heidelberg, Germany, 2006.
60. Joe, H. *Dependence Modeling with Copulas*; CRC Press: Boca Raton, FL, USA, 2014.
61. Zhang, L.; Singh, V.P. Bivariate Rainfall and Runoff Analysis Using Entropy and Copula Theories. *Entropy* **2012**, *14*, 1784–1812. [CrossRef]
62. Pirani, F.J.; Najafi, M.R. Multivariate Analysis of Compound Flood Hazard Across Canada's Atlantic, Pacific and Great Lakes Coastal Areas. *Earths Future* **2022**, *10*, e2022EF002655. [CrossRef]
63. Frahm, G.; Junker, M.; Schmidt, R. Estimating the tail-dependence coefficient: Properties and pitfalls. *Insur. Math. Econ.* **2005**, *37*, 80–100. [CrossRef]
64. Salvadori, G.; De Michele, C. Multivariate multiparameter extreme value models and return periods: A copula approach. *Water Resour. Res.* **2010**, *46*, 10. [CrossRef]
65. Fisher, N.I.; Switzer, P. Graphical assessment of dependence: Is a picture worth 100 tests? *Am. Stat.* **2001**, *55*, 233–239. [CrossRef]
66. Killiches, M.; Kraus, D.; Czado, C. Using model distances to investigate the simplifying assumption, model selection and truncation levels for vine copulas. *arXiv* **2016**, arXiv:1610.08795.